JACS
JOURNAL OF THE AMERICAN CHEMICAL SOCIETY
Article
pubs.acs.org/JACS

Enzyme-Catalyzed Oxidation Facilitates the Return of Fluorescence for Single-Walled Carbon Nanotubes

Cheuk Fai Chiu,[†] Brian A. Barth,[†] Gregg P. Kotchey,[†] Yong Zhao,[†] Kristy A. Gogick,[†] Wissam A. Saidi,[‡] Stéphane Petoud,[†,§] and Alexander Star*[,†]

[†]Department of Chemistry, University of Pittsburgh, Pittsburgh, Pennsylvania 15260, United States
[‡]Department of Chemical and Petroleum Engineering, University of Pittsburgh, Pittsburgh, Pennsylvania 15261, United States
[§]Centre de Biophysique Moléculaire, 45071 Cedex 2 Orléans, France

Supporting Information

ABSTRACT: In this work, we studied enzyme-catalyzed oxidation of single-walled carbon nanotubes (SWCNTs) produced by the high-pressure carbon monoxide (HiPco) method. While oxidation via strong acids introduced defect sites on SWCNTs and suppressed their near-infrared (NIR) fluorescence, our results indicated that the fluorescence of SWCNTs was restored upon enzymatic oxidation, providing new evidence that the reaction catalyzed by horseradish peroxidase (HRP) in the presence of H_2O_2 is mainly a defect-consuming step. These results were further supported by both UV−vis−NIR and Raman spectroscopy. Therefore, when acid oxidation followed by HRP-catalyzed enzyme oxidation was employed, shortened (<300 nm in length) and NIR-fluorescent SWCNTs were produced. In contrast, upon treatment with myeloperoxidase, H_2O_2, and NaCl, the oxidized HiPco SWCNTs underwent complete oxidation (i.e., degradation). The shortened, NIR-fluorescent SWCNTs resulting from HRP-catalyzed oxidation of acid-cut HiPco SWCNTs may find applications in cellular NIR imaging and drug delivery systems.

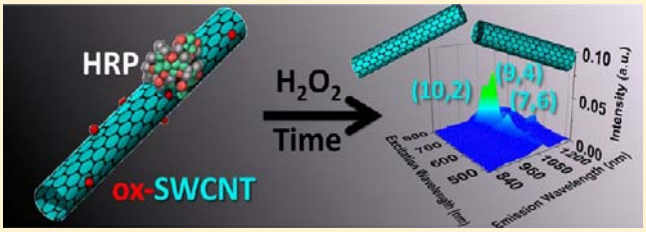

INTRODUCTION

Because of the unique properties of carbon nanotubes (CNTs), such as their small size, large surface area, high strength, ability to transport electrons, and inert chemical nature, this carbon-based nanomaterial has been incorporated in a wide array of applications, including building composites, electronics, and medical therapeutics.[1−3] The full implementation of CNTs in consumer goods, however, may be hindered as a result of emerging evidence that this nanomaterial can induce cytotoxic effects such as inflammation, epithelioid granulomas, fibrosis, and oxidation stresses that stem from both the chemical/electronic properties and the fibrous, anisotropic geometry of CNTs.[4,5] Moreover, CNTs that are engulfed by cells during endocytosis may rupture the cell membrane as a result of their length;[5] therefore, there is a direct correlation between cytotoxic response and CNT length. A recent study by Ali-Boucetta et al.[6] has also demonstrated that the toxicity of CNTs is dependent on both their lengths and surface functionalities imparted to this nanomaterial. For this reason and as a result of better circulation,[7,8] shortened CNTs, which are generally fabricated through chemical oxidation, have been employed for in vitro and in vivo drug delivery applications.[9,10] The primary shortcomings of employing harsh chemical oxidation methods to shorten (i.e., "cut") the length of semiconducting single-walled carbon nanotubes (s-SWCNTs) entails damaging the sp^2 lattice and creating oxygen functionalities, both of which result in the loss of the nanotubes' intrinsic near-infrared (NIR) fluorescence.[11,12]

Recently, we and others have demonstrated that peroxidases such as the plant-derived enzyme horseradish peroxidase (HRP)[13−18] and myeloperoxidase (MPO),[18−21] an enzyme expressed by inflammatory cells in humans, can oxidatively degrade CNTs and graphene oxide. HRP is obtained from the root of the horseradish plant and contains 308 amino acid residues and an iron(III) protoporphyrin IX heme active site. In the presence of H_2O_2, this enzyme can oxidize organic substrates[22,23] and carbon-based nanomaterials,[13−18] including SWCNTs. After reaction with H_2O_2, the oxidation state of the iron atom in the heme group is increased from (III) to (IV), and a porphyrin-based radical cation is formed. The iron(IV) porphyrin radical cation state of the enzyme, known as Compound I, oxidizes a substrate by two sequential one-electron oxidation steps, whereby Compound I is reduced to Compound II and subsequently back to the native iron(III) form of HRP; this process is called the peroxidase cycle.[24] The presence of oxygen functionalities on the carbon nanomaterial may also influence the ability of HRP to oxidize the substrate. For example, it has been demonstrated that attractive electrostatic interactions between negatively charged carboxyl functional groups on the surface of a SWCNT and the

Received: January 25, 2013
Published: May 15, 2013

   dx.doi.org/10.1021/ja400699y | J. Am. Chem. Soc. 2013, 135, 13356−13364

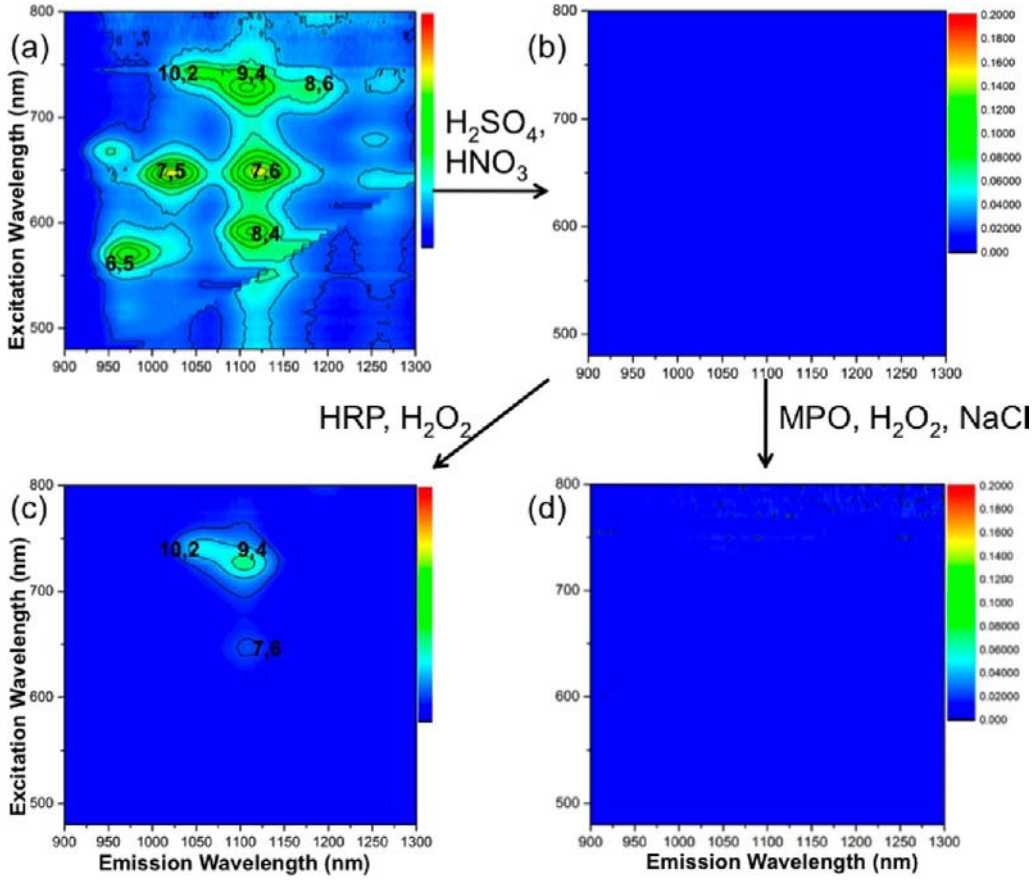

Figure 1. Photoluminescence (PL) maps of SWCNTs (a) before and (b) after acid oxidation and of the acid-oxidized SWCNT sample from (b) after treatment with (c) HRP/H_2O_2 or (d) MPO/H_2O_2/NaCl. Prior to PL mapping, sodium cholate (1 wt %) was added, and the samples were sonicated for 2 h. Literature values were employed to assign the SWCNT chirality.[25]

positively charged arginine residues of HRP may decrease the distance between the SWCNT and the reactive heme site of HRP, thereby permitting oxygen-functionalized SWCNTs (but not pristine SWCNTs, which do not possess these negatively charged functional groups) to undergo further oxidation.[14] MPO, a 144 kDa protein dimer that also contains two heme groups, acts in the same way as HRP, except in the presence of chloride (Cl^-); MPO is known to react with H_2O_2 and Cl^- to yield hypochlorite (ClO^-), which is the major oxidant responsible for the degradation of nanomaterials.[19,20]

In this work, we extended our study of enzymatic oxidation to SWCNTs synthesized by the high-pressure carbon monoxide (HiPco) method because the small diameter of these nanotubes enables one to probe the material's electronic properties and chirality distribution using photoluminescence (PL) mapping.[25] While oxidation via strong acids introduces defect sites on SWCNTs and suppresses their NIR fluorescence, our results indicated that the NIR fluorescence of certain types of SWCNTs is restored upon enzymatic oxidation, providing new evidence that the oxidation reaction catalyzed by HRP in the presence of H_2O_2 occurs at the defect sites. When acid oxidation followed by HRP-catalyzed enzyme oxidation was employed, shortened (<300 nm in length) and NIR-fluorescent SWCNTs were produced. The resulting products could find applications in NIR imaging and drug delivery systems.

RESULTS

Figure 1 presents PL maps of SWCNTs at various stages of oxidation. The typical characteristic band-gap luminescence was assigned to SWCNT chirality according to the literature.[25] The emissions were disrupted upon acid oxidation (Figure 1a,b);[11,12] upon HRP/H_2O_2 treatment, however, the fluorescence returned to the SWCNTs with certain chiralities [i.e., (9,4), (10,2), and (7,6); Figure 1c]. This was not observed for the MPO/H_2O_2/NaCl system (Figure 1d).

For pristine SWCNTs, four major peaks were determined in the radial breathing mode (RBM) section of the Raman spectra (i.e., at 196, 217, 258, and 283 cm^{-1}). Upon acid oxidation, the 283 cm^{-1} peak was fully suppressed (Figure 2a, left). A similar result was also reported by Yang et al.,[26] who attributed the loss of signal to the destruction of smaller-diameter SWCNTs during the acid oxidation. The D-band/G-band (D/G) ratio decreased from 0.51 for acid-oxidized SWCNTs to 0.24 for acid-oxidized SWCNTs treated with HRP/H_2O_2 (Figure 2a, right). Likewise, a decrease in the D/G ratio was observed for the MPO/H_2O_2/NaCl-treated SWCNTs (Figure 2b, right); this decrease to 0.27, however, was likely the result of nanotube degradation. Further evidence of degradation was provided by the decrease in the RBM and G-band signals, which possibly stemmed not only from the loss of resonance as the sp^2 surface was damaged but also from a high fluorescence background arising from organic fragments.[17,27]

UV−vis−NIR absorption spectra of the samples before oxidation, after acid oxidation, and after enzymatic treatment

dx.doi.org/10.1021/ja400699y | J. Am. Chem. Soc. 2013, 135, 13356−13364

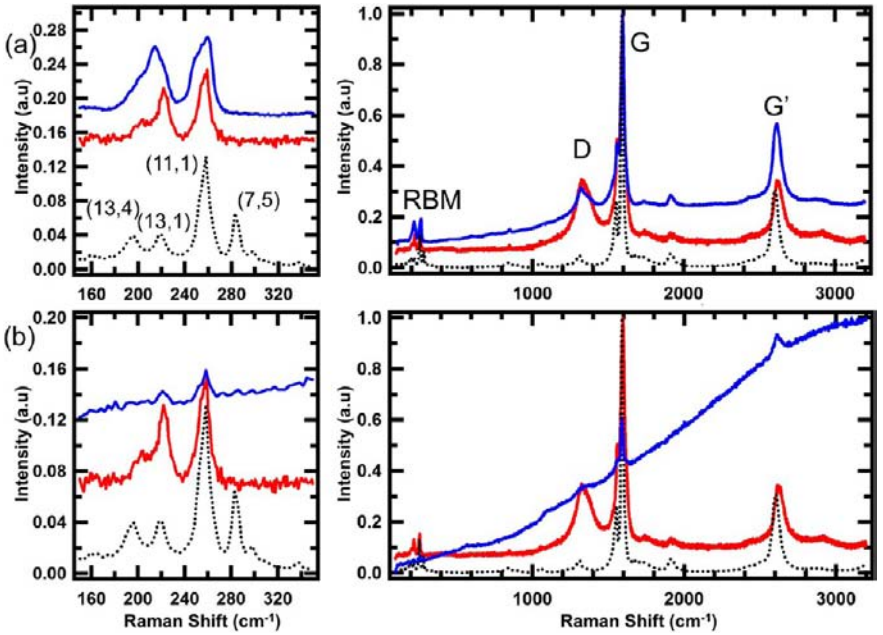

Figure 2. Enlarged radial breathing mode (RBM) sections and the full Raman spectra of SWCNTs treated with (a) HRP/H_2O_2 and (b) MPO/H_2O_2/NaCl at various experimental stages [before oxidation (black, dotted), after acid oxidation (red), and after enzymatic reaction (blue)]. The SWCNT chirality was assigned according to the literature.[28] The RBM sections have been offset for clarity.

are presented in Figure 3. The S_{11} (900−1600 nm) and S_{22} (600−900 nm) optical transitions for the semiconducting nanotubes, which were clearly present before oxidation, disappeared after acid oxidation and then reappeared after HRP/H_2O_2 treatment (Figure 3a), which is all in agreement with the PL results. On the other hand, upon MPO/H_2O_2/NaCl treatment, the overall absorbance of the SWCNTs decreased by ∼50% (Figure 3b); such a loss in absorbance can be attributed to the loss of carbon content.[19]

The spectroscopy results were further supported by transmission electron microscopy (TEM) images of the SWCNT samples. Figure 4 indicates that the SWCNT bundles were shortened by 35% during the acid treatment (Figure 4b). High-resolution TEM (HRTEM) imaging of the acid-oxidized SWCNTs (Figure 4c) revealed both significant bundling of SWCNTs and a rough/defective sidewall structure. The TEM image of the acid-oxidized SWCNTs treated with MPO/H_2O_2/NaCl (Figure 4d) revealed only carbonaceous fragments, which are the typical products of the degradation process.[13,16,17,19,29] As tubular objects were not present in the image, a histogram for this sample was not recorded. In contrast, after HRP/H_2O_2 treatment (Figure 4e), a 30% reduction in bundle length was observed. The average length of the HRP/H_2O_2-treated SWCNT bundles was 215 ± 125 nm. In the HRTEM image (Figure 4f), this sample appeared to be less bundled and demonstrated a more defined CNT sidewall structure.

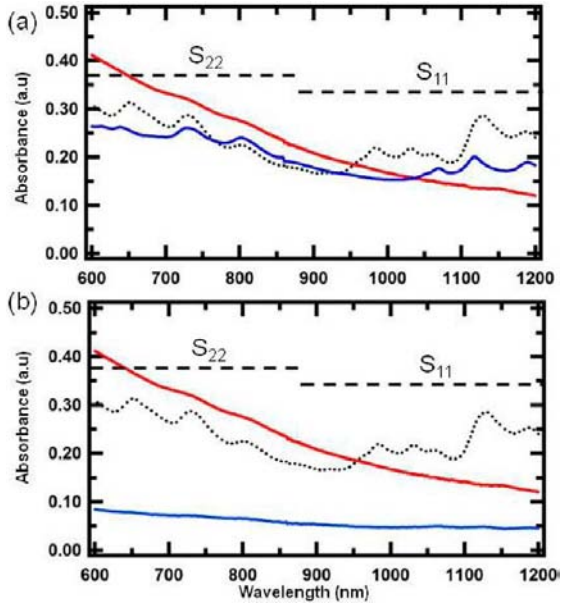

Figure 3. UV−vis−NIR absorption spectra of SWCNTs treated with (a) HRP/H_2O_2 and (b) MPO/H_2O_2/NaCl at various experimental stages [before oxidation (black, dotted), after oxidation (red), and after enzymatic reaction (blue)].

DISCUSSION

The enzyme-catalyzed oxidation of acid-treated SWCNTs revealed some interesting chiral selectivity, as demonstrated in Figure 1c. To identify the chiralities of these nanotubes, PL results were cross-examined with the Raman RBM data. From our PL maps (Figure 1c), the (10,2), (7,6), and (9,4) nanotubes were identified, but the Raman spectra demonstrated an absence of the (10,2) species (Figure 2). We hypothesize that these seemingly contradictory results stemmed from the fact that the S_{22} absorbance bands of (10,2) s-SWCNTs, which have corresponding wavelengths of 733 nm, were out of resonance with the excitation laser (i.e., 633 nm), thereby resulting in the absence of their Raman signal.[28] From the Raman RBM spectrum of the pristine SWCNTs, four major peaks were located at ∼196, 217, 258, and 283 cm^{-1} (Figure 2, black dotted trace). Further fitting of the RBM data utilizing Lorentzian functions revealed that the four peaks corresponded mainly to (13,4), (13,1), (11,1), and (7,5) SWCNTs, respectively, of which the former two are metallic and lack PL properties, whereas the latter two are semiconducting.[30] It is also interesting to note that the RBMs for the metallic

dx.doi.org/10.1021/ja400699y | J. Am. Chem. Soc. 2013, 135, 13356−13364

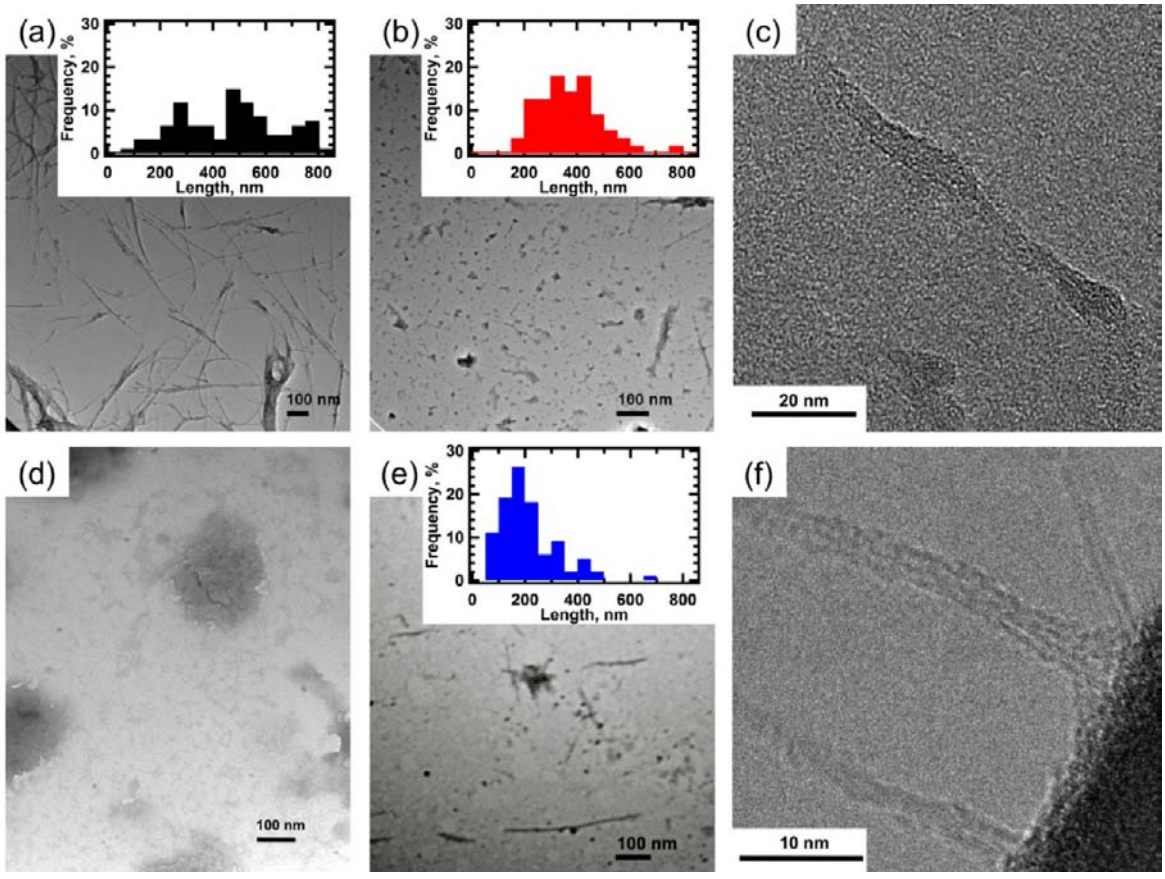

Figure 4. (a,b) Transmission electron microscopy (TEM) micrographs of SWCNT bundles (a) before and (b) after acid oxidation. (c) High-resolution TEM (HRTEM) image of the acid-oxidized SWCNT bundles. (d,e) TEM micrographs of the acid-oxidized SWCNT bundles after treatment with (d) MPO/H_2O_2/NaCl or (e) HRP/H_2O_2. (f) HRTEM micrograph of the HRP/H_2O_2-treated sample. The insets in (a), (b), and (e) depict histograms of the length distributions for the SWCNT bundles at various experimental stages.

SWCNTs were upshifted by ~10 cm^{-1} upon acid oxidation; such an upshift, however, was not observed for the semiconducting SWCNTs at 258 cm^{-1}. While the possible causes of this upshift are still debatable, with reasons ranging from bundling-induced red shifts of transition energies[31,32] to charge transfer from SWCNTs to −COOH groups,[33] the fact that metallic SWCNTs shifted more than their semiconducting counterparts agrees with a previous report that metallic tubes are more reactive than semiconducting SWCNTs in the 0.9−1.1 nm diameter range.[26] The observed upshift was reversed upon HRP/H_2O_2 treatment, which is similar to what has been reported for oxidized SWCNTs upon annealing.[34]

Meanwhile, the Raman signal for the (7,5) SWCNTs was absent after the acid treatment, and their fluorescence did not return after incubation with HRP/H_2O_2 (Figure 1c), suggesting that the (7,5) nanotubes were destroyed during the acid treatment process.[26]

The observed decreases in the Raman D/G ratio appeared similar to the data obtained for enzyme-catalyzed oxidation of multiwalled CNTs.[16] While a decrease in the D/G ratio can be interpreted as a decrease in defect density, as demonstrated by Strano and co-workers,[35] this change could also result from decreases in both the D and G bands at high degrees of functionalization due to the loss of resonance enhancement. Therefore, a decrease in the D/G ratio alone is not a conclusive way to show a decrease in defect density.[36] As a result, UV−vis−NIR and PL spectroscopy were also utilized to provide insight into the defect density of oxidized SWCNTs. Such a degradation-induced decrease in the D/G ratio was exhibited by the oxidized SWCNTs upon MPO/H_2O_2/NaCl treatment and will be discussed later.

Functionalized SWCNTs are known to exhibit a flattened UV−vis−NIR absorbance spectra[37] and no NIR fluorescence[30] because the introduced defect sites disrupt the electronic structure of the nanotubes. Such behavior was demonstrated by the acid-treated SWCNTs (Figures 1b and 3). The opposite trend, however, was observed upon enzymatic oxidation via HRP/H_2O_2, where the UV−vis−NIR signal and NIR fluorescence were restored (Figure 1c and 3a); these results are similar to those reported for Ar annealing.[38] Our PL map for the acid-treated SWCNT sample after the HRP/H_2O_2 reaction revealed the presence of (10,2), (7,6), and (9,4) nanotubes; their corresponding absorption bands were also present on the UV−vis−NIR absorption spectrum (Figure 3a, blue trace). Combining our Raman and optical results, we concluded that the HRP/H_2O_2 reaction specifically attacked defect sites and restored the sp^2 lattice.

In Figure 1c, the emission wavelength (λ_{em}) for oxidized (7,6) SWCNTs that were treated with HRP/H_2O_2 was blue-shifted by ~14 nm (i.e., from ~1122 to ~1108 nm). In contrast, when a duplicate experiment was performed, acid-oxidized SWCNTs that were treated with HRP/H_2O_2 did not demonstrate any blue shift (Figure S2 in the Supporting Information). We attribute these apparently contradictory results to differences in the local environments.[39] Also, for both sets of data, the same restoration of emission was

dx.doi.org/10.1021/ja400699y | J. Am. Chem. Soc. 2013, 135, 13356−13364

observed for (9,4), (8,6), and (7,6) chiralities with the removal of (6,5), (7,5), and (8,4) species (Figure S2), which is consistent with previous studies showing that acid treatment removes SWCNTs with diameters smaller than 0.88 nm [i.e., (8,6) SWCNTs have a diameter of 0.966 nm].[26,28] Finally, the peak due to (8,6) SWCNTs was more intense in the duplicate experiment.

We attributed these results to the removal of defect sites (most likely oxygen-containing functional groups) from the surfaces of SWCNTs. The data presented herein indicate that HRP/H_2O_2 oxidized the functionalized SWCNTs through reactive intermediates of the peroxidase cycle, thereby removing oxygen groups and restoring the sp^2 lattice, possibly through decarboxylation.[14,16,17,40] As suggested by Kane and colleagues, the removal of a carboxyl group involves breaking only the one intact bond connecting it to the CNT backbone, whereas removal of hydroxyl, epoxide, and peroxides groups requires breaking three backbone bonds.[41] Therefore, decarboxylation would be more energetically favorable than oxidation and eventual removal of other oxygen-containing functional groups.[41] Our work, however, does not suggest any further oxidation of the graphitic lattice of the nanotube after the enzymatic reaction. Instead, our Raman D/G ratio, UV–vis–NIR absorbance, and PL map data all indicate a reduction in the number of defect sites and a restoration of the sp^2 lattice.

To exclude the possibility that the return of the PL emission resulted from the reduction of oxygen functional groups via the oxidase cycle of HRP,[24] a control experiment was performed wherein oxidized SWCNTs were incubated in the absence of H_2O_2 for 35 days. Under our experimental conditions, no PL emission characteristic of SWCNTs was observed (Figure S3 in the Supporting Information), thereby indicating that oxidation via the peroxidase cycle rather than reduction via the oxidase cycle is the likely mechanism for the return of fluorescence.

Density functional theory (DFT) calculations were performed to estimate the overall energy change for decarboxylation of a SWCNT containing both a carboxyl group and an adjacent ketone group (Figure 5). To estimate the overall energy for decarboxylation of a (14,0) SWCNT functionalized with both a carboxyl group and a ketone group, the nudged elastic band (NEB) method was used to determine the minimum-energy path for the following reaction:

$$\mathrm{SWCNT(=O)-COOH \rightarrow SWCNT-OH + CO_2(g)}$$

The reactant has a −COOH group and the oxygen of the ketone group adsorbed on a neighboring site of a sidewall ring, as shown schematically in the upper left inset in Figure 5b. The functionalization locally disrupts the π-orbital network of the tube. The products correspond to the complete decarboxylation of the oxidized SWCNT, resulting in the formation of a hydroxyl group on the nanotube and carbon dioxide in the gas phase.[14] As can be seen in Figure 5b, the decarboxylation process proceeds with a small energy barrier of 0.15 eV. In the transition state (upper right inset in Figure 5b), the hydrogen of the −COOH group rotates from the optimum position towards the oxygen of the ketone group. It is also noteworthy that the decarboxylation process is exothermic and thermodynamically very favorable, with an energy release of ~2.9 eV per desorbed CO_2 molecule in the gas phase.

Although the employed SWCNT model is idealized, as it ignores the presence of defects, it nevertheless reveals that the decarboxylation is thermodynamically very favorable under the experimental conditions. To show that this is also the case even

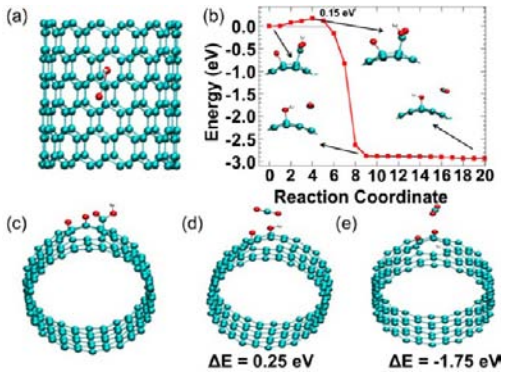

Figure 5. (a) Top view of a COOH-functionalized (14,0) SWCNT. (b) Reaction energy profile for the decarboxylation of a pristine (14,0) SWCNT functionalized with a carboxyl group and a ketone group. The insets show side views of selected parts of the SWCNT for the (upper left) initial, (upper right) transition-state, and (lower left and right) final configurations during the decarboxylation process. The potential energy surface near the final state is very flat because of the small energy barrier for the rotation of −OH group around the O–C bond, as can be seen by inspecting the lower two insets. (c) Initial and (e) final configurations for the decarboxylation of a defective (14,0) CNT functionalized with a −COOH group and two ketone groups. This process is exothermic by 1.75 eV per CO_2 molecule. (d) Structure of a possible intermediate transition state in which the hydrogen of the −COOH group is transferred to the ketone group to form an −OH group with the release of CO_2 in the gas phase. Carbon atoms are turquoise, oxygen atoms are red, and hydrogen atoms are white.

in the presence of CNT defects, we examined the energetics of possible initial and final structures in the decarboxylation process. This is shown in Figure 5c,e for a (14,0) SWCNT with a carbon vacancy that is functionalized with −COOH group and two ketone groups. As in the case of the pristine SWCNT, the decarboxylation process for the CNT with the defect is also exothermic by ~1.75 eV per desorbed CO_2 molecule in the gas phase. The configuration shown in Figure 5d is a potential transition state for this process that is only 0.25 eV higher in energy than the initial structure. In the presence of a solvent, as is the case in the experiments, this transition state would be expected to have a lower energy because a proton could be transferred from solution to passivate the dangling bond of the CNT that is left by the desorbed CO_2 molecule.

The decarboxylation process was also evidenced in a control experiment wherein pristine HiPco SWCNTs were subjected to HRP/H_2O_2 oxidation. They demonstrated an improved UV–vis–NIR and NIR fluorescence signal as well as a decrease in the Raman D/G ratio (Figure S4 in the Supporting Information). Recent research has suggested that defect sites are present in pristine HiPco SWCNTs, constraining the fluorescence to ~40% of its maximum brightness.[42] Therefore, HRP/H_2O_2 oxidation may remove defect sites on pristine SWCNTs just as this enzymatic system removes defect sites on the oxidized samples.

The MPO/H_2O_2/NaCl reaction is known to produce hypochlorite (ClO^-), which is the strongest oxidant of the MPO system.[19,20] ClO^- oxidizes the sidewalls of SWCNTs, which in turn damages the sp^2 network and results in loss of the resonance condition for the Raman response. In comparison with the HRP/H_2O_2 reaction, the MPO/H_2O_2/NaCl system demonstrated no return of fluorescence, suggesting a different oxidation mechanism that does not involve the restoration of

dx.doi.org/10.1021/ja400699y | J. Am. Chem. Soc. 2013, 135, 13356–13364

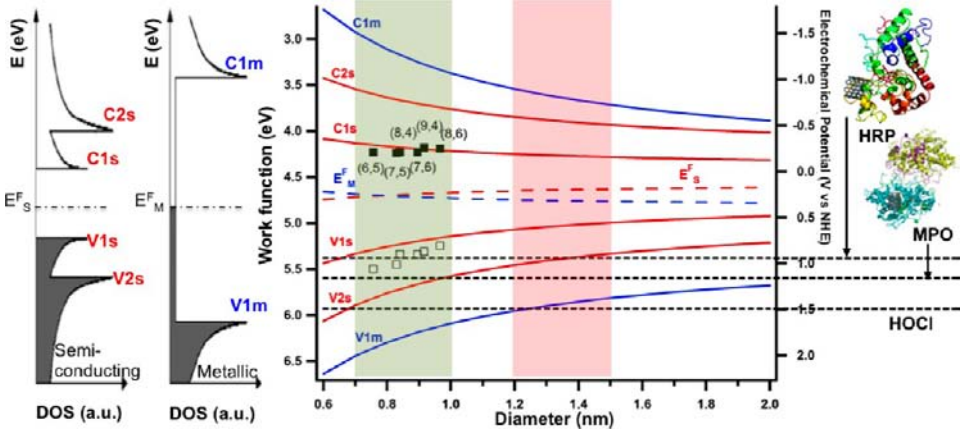

Figure 6. Electrochemical potentials of valence (V) and conduction (C) bands of semiconducting (s) SWCNTs (red curves) and metallic (m) SWCNTs (blue curves) as functions of SWCNT diameter. The density of states (DOS) diagrams at the left indicate the various bands. The corresponding Fermi energies (E^F) are shown as long-dashed lines. The oxidation potentials of HRP, MPO, and HOCl are indicated by black short-dashed lines. The dependence of the electrochemical potentials of SWCNTs on their diameter was modeled in ref 45 with experimental data adapted from ref 46 (squares). The green-shaded region indicates the diameter range of the smaller-diameter HiPco SWCNTs studied in this work. The pink-shaded region indicates the larger-diameter SWCNTs utilized in earlier work.[13,14] The HRP, MPO, and HOCl potentials were adapted from ref 18. The structures showing possible binding positions of HRP and MPO with carboxylated SWCNTs (right) were adapted from refs 14 and 19, respectively. The DOS diagrams were adapted from ref 47.

the sp^2 surfaces. Therefore, the acid-treated SWCNTs were likely degraded by the MPO/H_2O_2/NaCl system, as evidenced by the fragment-induced fluorescence in the Raman spectrum (Figure 2b),[17,27] the loss of overall UV–vis–NIR absorption (Figure 3b),[19,20] and the fragmented byproducts visualized by TEM (Figure 4d).

Pristine SWCNTs were also subjected to the MPO/H_2O_2/NaCl system. After the five day treatment, however, no degradation was observed for the pristine SWCNTs (Figure S5 in the Supporting Information); we believe this observation to be a consequence of insufficient production of ClO^- with the current experimental setup. In a different control experiment (Figure S6 in the Supporting Information), pristine SWCNTs were incubated with 0.20 M NaClO; the SWCNTs were destroyed within 1 day, thereby providing evidence that high concentrations of ClO^- can degrade even pristine SWCNTs.

In comparison with earlier work on HRP/H_2O_2 oxidation of larger-diameter SWCNTs,[13,14] the smaller-diameter HiPco SWCNTs degraded at a lower rate. The complete degradation of CNTs by the HRP/H_2O_2 system after ~30 days at room temperature has been reported.[14,16,17] Since oxygen-containing defects were found to be essential for this enzymatic oxidation,[14,16,17] one might expect the defect density to be higher for the larger-diameter SWCNTs than the SWCNTs used in this work, where the lower defect density would be responsible for the lower reaction rate. To test this hypothesis, the defect density was determined by the acid titration method following a published procedure.[16,43] The density of oxygen-containing defects for the SWCNTs used in this work was calculated to be 7.8 ± 0.5 μmol/mg, versus 3.4 ± 0.2 μmol/mg for the larger-diameter SWCNTs used before. This affirmed that the defect density was not the reason for the difference in the degradation rates as the smaller-diameter SWCNTs had both a higher defect density and a lower rate than their larger-diameter counterparts. Although this defect density of 7.8 ± 0.5 μmol/mg is an average value for SWCNTs of all chiralities in the sample and it is likely that some SWCNTs (e.g., metallic tubes) are more defective than others, as reported in the literature,[26] the difference in our results cannot be solely explained by defect density.

Selectivity by the redox potential of SWCNTs has been suggested and utilized by O'Connell et al.[44] Similar reasoning was constructed by us to explain the oxidation by HRP, MPO, and HOCl.[18] Recently, the redox potentials of SWCNTs with different chiralities and diameters were modeled[45] and experimentally measured[46] via electrochemistry coupled with spectroscopy. Figure 6 shows the electrochemical potentials of various bands of SWCNTs as functions of nanotube diameter (red and blue curves) along with the oxidation potentials of HRP, MPO, and HOCl (black dashed lines).[18,44] The electrochemical potential of the s-SWCNT valence band (V1s) has been shown to increase as the nanotube diameter decreases (Figure 6). In this model, electron transfer takes place from the top of the valence band to the oxidizing species. The redox potential of HRP/H_2O_2 is ~0.95 V, which is higher than that of the V1s band of the larger-diameter SWCNTs (pink-shaded region in Figure 6) but similar to that of the smaller-diameter SWCNTs (green-shaded region). As a result of this difference in the redox potential, larger-diameter SWCNTs are more favorably oxidized than smaller-diameter SWCNTs, in agreement with the shortened degradation time that we observed for larger SWCNTs.[14,16] For the MPO/H_2O_2/NaCl system, HOCl is produced; it has a redox potential of 1.48 V,[18] which represents a much higher oxidizing capacity than for HRP. At this potential, HOCl has a significant potential difference even with smaller-diameter SWCNTs and therefore oxidizes them, as evidenced by the degradation of the acid-treated HiPco SWCNTs by the MPO/H_2O_2/NaCl system. Furthermore, the fact that smaller-diameter pristine SWCNTs, which cannot be degraded by HRP/H_2O_2 (Figure S4 in the Supporting Information), were degraded by hypochlorite ions (Figure S5 in the Supporting Information) also supports the electrochemical potential argument.

While this model works well for pristine SWCNTs, they are often p-doped by acid treatment,[33] which further increases their redox potential and theoretically lowers their reactivity compared with the pristine SWCNTs by drawing their valence

dx.doi.org/10.1021/ja400699y | J. Am. Chem. Soc. 2013, 135, 13356–13364

band closer to the oxidation potential of the reactive species. This may not be the case, however, as pristine SWCNTs were shown not to be degradable by enzymatic oxidation.[14,16] Therefore, certain functionalities are required for the SWCNTs to undergo the peroxidase cycle. Carboxyl and hydroxyl (phenol) groups have labile hydrogen atoms that assist the peroxidase cycle, in which Compound I oxidizes a substrate by two sequential one-electron oxidation steps to form water. In pristine SWCNTs that have neither functional groups nor labile hydrogen atoms, the biodegradation of pristine SWCNTs cannot be initiated.

On the basis of our results, HPR/H_2O_2 oxidation results in restoration of the fluorescence of SWCNTs, indicating a chemical pathway in which functional groups are eliminated in order to restore the sp^2 lattices of the nanotubes. Such a pathway was not observed for the MPO/H_2O_2/NaCl and NaOCl systems. From the degradation of pristine SWCNTs by NaOCl, it appears that the hypochlorite ions directly attack the sidewalls of the SWCNTs.

CONCLUSION

HRP/H_2O_2 can oxidize highly defective, carboxylated SWCNTs and restore their optical properties. To this end, SWCNTs that were oxidized by a strong acid mixture and demonstrated weak absorption bands with no photoluminescence were further oxidized using HRP/H_2O_2 to yield shorter, less defective CNTs with well-defined absorption bands and a strong PL signal. HRP may be capable of oxidizing only carboxylic acid groups, which would be removed from the CNT lattice as CO_2.[14,16,17] It is possible that other oxygen-containing functional groups such as hydroxyl, epoxide, and peroxides groups are not as easily removed from the lattice as carboxylic groups because of the numbers of bonds between the carbon in the oxygen functional group and the lattice.[41] In contrast, when treated with MPO/H_2O_2/NaCl, the oxidized HiPco SWCNTs underwent complete oxidation (i.e., degradation) as a result of the highly oxidative reagent, ClO^-. The shortened, fluorescent SWCNTs produced by HRP/H_2O_2 may find applications as NIR imaging agents or nanocarriers for use in medical diagnostics and therapeutics.

MATERIALS AND METHODS

Chemical Oxidation. Purified HiPco SWCNTs[38,48] were purchased from NanoIntegris, Inc. (Skokie, IL). SWCNTs (10 mg) were sonicated in sulfuric acid (Fisher Scientific)/nitric acid (J.T. Baker) solution (15 mL of H_2SO_4, 5 mL of HNO_3) for 3 h 50 min at 40 °C. The oxidized SWCNT sample was diluted with deionized (DI) water, vacuum-filtered, washed with DI water several times, and collected on separate polytetrafluoroethylene (PTFE) filter papers to form thin films, known in the literature as buckypaper.[49] Pieces of the buckypaper were cut and redispersed in DI water by sonication for 40 min at room temperature. The resulting suspensions were centrifuged (3500 rpm, 20 min), and the supernatant was collected for enzymatic oxidation.

Enzymatic Oxidation of SWCNTs Using HRP. The procedure for the enzymatic oxidation of SWCNTs with HRP/H_2O_2 has been described elsewhere.[13,14,16] Briefly, 8 mL of the supernatant containing oxidized SWCNTs was combined with 1.5 mg of HRP (Sigma-Aldrich). The sample was incubated for 24 h at room temperature on a shaker in the absence of light. After the incubation period, 4 μL of H_2O_2 (0.089 M, Sigma-Aldrich) was added daily to the oxidized SWCNT sample for 35 days. The sample was incubated with continuous shaking during this period. In a separate control experiment, nonoxidized SWCNTs were treated with 1.5 mg of HRP/H_2O_2 employing the same method. Both samples were characterized after 35 days using UV−vis−NIR spectroscopy, TEM, Raman spectroscopy, and PL mapping.

Enzymatic Oxidation of SWCNTs Using MPO. The protocol for enzymatic oxidation catalyzed by MPO was adopted from Kagan et al.,[19] with the total volume scaled for spectrometer requirements. Lyophilized purified native human MPO was purchased from Athens Research and Technology, Inc. (Athens, GA) and reconstituted with 350 μL of nanopure water to give a final concentration of 2.0 μM. Sodium chloride, diethylenetriaminepentaacetic acid (DTPA), and 0.1 M phosphate buffer were purchased from Sigma-Aldrich. A 100 μL aliquot of the oxidized SWCNT supernatant solution was mixed with 21 μL of 5 M NaCl, 45 μL of 5 mM DTPA, 12 μL of MPO solution, 4 μL of 18.75 mM H_2O_2, and 568 μL of 0.1 M phosphate buffer. Every hour, 4 μL of 18.75 mM H_2O_2 was added for a total of seven additions a day for 5 days. The MPO solution was added to the mixture at a rate of 12 μL/day to compensate for the loss of enzyme activity in the incubation system. The sample was characterized after 5 days using UV−vis−NIR spectroscopy, TEM, Raman spectroscopy, and PL mapping. In a separate control experiment, nonoxidized SWCNTs were treated with MPO/H_2O_2/NaCl under the same conditions. In a different control experiment, pristine SWCNTs were incubated with 0.20 M NaClO for 1 day to explore the effect of high NaClO concentrations on SWCNT degradation.

Raman Spectroscopy. SWCNTs were excited with a 633 nm laser, and measurements were performed using a Renishaw InVia Raman microscope (Wotton-under-Edge, UK). Aliquots (~0.1 mL) of suspended SWCNTs were drop-cast on a glass slide and allowed to dry under ambient conditions overnight, thereby forming aggregates of SWCNTs. Scans were carried out at a laser power of 1.7 mW with an accumulation time of 10 s over the range from 100 to 3200 cm^{-1}. Spectra were acquired from multiple locations on the SWCNT aggregates, and the results were normalized to the most intense peak and averaged in accordance with published procedures.[50]

TEM Imaging and Histogram Determination. A suspension of dispersed SWCNTs (6 μL) was diluted by a factor of 100, drop-cast onto carbon-coated lacey copper grids (Pacific Grid-Tech, San Francisco, CA), and allowed to dry overnight. Analysis was performed using a Morgagni transmission electron microscope (FEI, Hillsboro, OR) with an 80 keV electron beam. The mean SWCNT length distributions were derived from the TEM micrographs for ~100 nanotubes per sample.

HRTEM Imaging. HRTEM images were obtained with a JEOL 2100F microscope at an accelerating voltage of 200 kV. TEM samples were evenly dispersed in aqueous solution. A 10 μL aliquot of each sample was drop-cast on an ultrathin carbon film/copper TEM grid (Ted Pella) and dried at room temperature overnight before being imaged.

UV−Vis−NIR Spectroscopy and PL Mapping. Sodium cholate was added to the SWCNT suspensions (pristine, acid-oxidized, HRP-treated, and MPO-treated) at a concentration of 1% (w/v), and the suspensions were sonicated for 2 h. UV−vis−NIR measurements of dispersed SWCNTs were acquired using a PerkinElmer Lambda 900 spectrophotometer over the wavelength range 200−1300 nm. PL maps were obtained using a Fluorolog 322 spectrofluorometer (HORIBA Jobin Yvon, Kyoto, Japan) equipped with a DSS-IGA020 L detector (Electro-Optical Systems, Phoenixville, PA). The excitation wavelength was scanned from 580 to 800 nm in 5 nm increments, and the emission was detected from 900 to 1300 nm in 2 nm increments. Spectra were corrected for variation in lamp intensity and monochromator response.

DFT Calculations. The quantum-chemical calculations of equilibrium geometries were carried out using the self-consistent-charge density-functional-based tight-binding (SCC-DFTB) method,[51] which has been successfully applied to a wide class of systems of interest, including CNTs.[52] As a validity check on our calculations, we found that the adsorption energy of COOH on (11,0) CNTs was 1.47 eV, which is in good agreement with the value of 1.42 eV obtained previously using standard DFT calculations. The minimum-energy paths were determined using the NEB method.[53] The calculations

were carried out using a periodic supercell approach with three repeat units of a (14,0) SWCNT sampled at the Γ point of the Brillouin zone.

Modified Boehm's Titration. A modified Boehm's titration procedure was utilized to determine the density of oxygen-containing functional groups on the surface of the acid-oxidized SWCNTs.[16,43] Approximately 3 mg of oxidized SWCNTs was dispersed in 6 mL of NaOH (Mallinckrodt) at 10 mM concentration. The sample was sealed with a septum stopper, sonicated, and degassed for 1.5 min under vacuum. The samples were incubated for 72 h. After the incubation process, the solutions were filtered through a 0.22 μm Teflon membrane. A small amount of the filtrate (0.25 mL) was transferred to a separate vial, to which was added 10 μL of aqueous indicator solution containing 3:2 (v/v) 0.1% bromocresol green and methyl red (Sigma Aldrich). The solution was titrated with 0.0082 M HCl (Fisher) using a pipet (Eppendorf). A blank control consisting of only NaOH was also treated using the same procedure to determine the concentration of NaOH. All of the titrations were repeated at least three times. The defect density (in units of μmol/mg) was calculated from the NaOH uptake by the SWCNTs divided by the mass. SWCNTs with larger diameters (∼1.4 nm) were purchased from Carbon Solutions, Inc. (Riverside, CA) and oxidized for 4 h using the same acid oxidation method. This sample was also characterized for defect density.

■ ASSOCIATED CONTENT

Supporting Information

Experimental procedure (Scheme S1), Lorentzian-fitted RBM region of the Raman spectrum of the pristine SWCNTs, extra DFT calculations for defective CNTs, AFM characterization, and spectroscopic data for control experiments (Figures S1–S8). This material is available free of charge via the Internet at http://pubs.acs.org.

■ AUTHOR INFORMATION

Corresponding Author

astar@pitt.edu

Notes

The authors declare no competing financial interest.

■ ACKNOWLEDGMENTS

The project described herein was supported by the National Institute of Environmental Health Sciences (Award R01ES019304). G.P.K. acknowledges support from EPA STAR Graduate Fellowship FP-91713801. K.A.G. acknowledges support from the Mary E. Warga Predoctoral Fellowship. S.P. acknowledges support from la Ligue contre le Cancer and Institut National de la Santé et de la Recherche Médicale (INSERM). The authors thank Tom Harper and NFCF for providing access to instrumentation.

■ REFERENCES

(1) Collins, P. G.; Avouris, P. *Sci. Am.* **2000**, *283*, 62.

(2) Fadel, T. R.; Look, M.; Staffier, P. A.; Haller, G. L.; Pfefferle, L. D.; Fahmy, T. M. *Langmuir* **2010**, *26*, 5645.

(3) Guldi, D. M.; Rahman, G. M. A.; Prato, M.; Jux, N.; Qin, S. H.; Ford, W. *Angew. Chem., Int. Ed.* **2005**, *44*, 2015.

(4) Lam, C.-w.; James, J. T.; McCluskey, R.; Arepalli, S.; Hunter, R. L. *Crit. Rev. Toxicol.* **2006**, *36*, 189.

(5) Shi, X. H.; von dem Bussche, A.; Hurt, R. H.; Kane, A. B.; Gao, H. J. *Nat. Nanotechnol.* **2011**, *6*, 714.

(6) Ali-Boucetta, H.; Nunes, A.; Sainz, R.; Herrero, M. A.; Tian, B.; Prato, M.; Bianco, A.; Kostarelos, K. *Angew. Chem., Int. Ed.* **2013**, *52*, 2274.

(7) Kolosnjaj-Tabi, J.; Hartman, K. B.; Boudjemaa, S.; Ananta, J. S.; Morgant, G.; Szwarc, H.; Wilson, L. J.; Moussa, F. *ACS Nano* **2010**, *4*, 1481.

(8) Murphy, F. A.; Poland, C. A.; Duffin, R.; Al-Jamal, K. T.; Ali-Boucetta, H.; Nunes, A.; Byrne, F.; Prina-Mello, A.; Volkov, Y.; Li, S. P.; Mather, S. J.; Bianco, A.; Prato, M.; MacNee, W.; Wallace, W. A.; Kostarelos, K.; Donaldson, K. *Am. J. Pathol.* **2011**, *178*, 2587.

(9) Liu, Z.; Sun, X. M.; Nakayama-Ratchford, N.; Dai, H. J. *ACS Nano* **2007**, *1*, 50.

(10) Chen, J.; Chen, S.; Zhao, X.; Kuznetsova, L. V.; Wong, S. S.; Ojima, I. *J. Am. Chem. Soc.* **2008**, *130*, 16778.

(11) Cognet, L.; Tsyboulski, D. A.; Rocha, J.-D. R.; Doyle, C. D.; Tour, J. M.; Weisman, R. B. *Science* **2007**, *316*, 1465.

(12) Dukovic, G.; White, B. E.; Zhou, Z.; Wang, F.; Jockusch, S.; Steigerwald, M. L.; Heinz, T. F.; Friesner, R. A.; Turro, N. J.; Brus, L. E. *J. Am. Chem. Soc.* **2004**, *126*, 15269.

(13) Allen, B. L.; Kichambare, P. D.; Gou, P.; Vlasova, I. I.; Kapralov, A. A.; Konduru, N.; Kagan, V. E.; Star, A. *Nano Lett.* **2008**, *8*, 3899.

(14) Allen, B. L.; Kotchey, G. P.; Chen, Y.; Yanamala, N. V. K.; Klein-Seetharaman, J.; Kagan, V. E.; Star, A. *J. Am. Chem. Soc.* **2009**, *131*, 17194.

(15) Russier, J.; Ménard-Moyon, C.; Venturelli, E.; Gravel, E.; Marcolongo, G.; Meneghetti, M.; Doris, E.; Bianco, A. *Nanoscale* **2011**, *3*, 893.

(16) Zhao, Y.; Allen, B. L.; Star, A. *J. Phys. Chem. A* **2011**, *115*, 9536.

(17) Kotchey, G. P.; Allen, B. L.; Vedala, H.; Yanamala, N.; Kapralov, A. A.; Tyurina, Y. Y.; Klein-Seetharaman, J.; Kagan, V. E.; Star, A. *ACS Nano* **2011**, *5*, 2098.

(18) Kotchey, G. P.; Hasan, S. A.; Kapralov, A. A.; Ha, S. H.; Kim, K.; Shvedova, A. A.; Kagan, V. E.; Star, A. *Acc. Chem. Res.* **2012**, *45*, 1770.

(19) Kagan, V. E.; Konduru, N. V.; Feng, W.; Allen, B. L.; Conroy, J.; Volkov, Y.; Vlasova, I. I.; Belikova, N. A.; Yanamala, N.; Kapralov, A.; Tyurina, Y. Y.; Shi, J.; Kisin, E. R.; Murray, A. R.; Franks, J.; Stolz, D.; Gou, P.; Klein-Seetharaman, J.; Fadeel, B.; Star, A.; Shvedova, A. A. *Nat. Nanotechnol.* **2010**, *5*, 354.

(20) Vlasova, I. I.; Sokolov, A. V.; Chekanov, A. V.; Kostevich, V. A.; Vasilyev, V. B. *Russ. J. Bioorg. Chem.* **2011**, *37*, 453.

(21) Shvedova, A. A.; Kapralov, A. A.; Feng, W. H.; Kisin, E. R.; Murray, A. R.; Mercer, R. R.; St. Croix, C. M.; Lang, M. A.; Watkins, S. C.; Konduru, N. V.; Allen, B. L.; Conroy, J.; Kotchey, G. P.; Mohamed, B. M.; Meade, A. D.; Volkov, Y.; Star, A.; Fadeel, B.; Kagan, V. E. *PLoS One* **2012**, *7*, e30923.

(22) Rota, C.; Fann, Y. C.; Mason, R. P. *J. Biol. Chem.* **1999**, *274*, 28161.

(23) Spadaro, J. T.; Renganathan, V. *Arch. Biochem. Biophys.* **1994**, *312*, 301.

(24) Berglund, G. I.; Carlsson, G. H.; Smith, A. T.; Szöke, H.; Henriksen, A.; Hajdu, J. *Nature* **2002**, *417*, 463.

(25) Bachilo, S. M.; Strano, M. S.; Kittrell, C.; Hauge, R. H.; Smalley, R. E.; Weisman, R. B. *Science* **2002**, *298*, 2361.

(26) Yang, C.-M.; Park, J. S.; An, K. H.; Lim, S. C.; Seo, K.; Kim, B.; Park, K. A.; Han, S.; Park, C. Y.; Lee, Y. H. *J. Phys. Chem. B* **2005**, *109*, 19242.

(27) Matousek, P.; Towrie, M.; Parker, A. W. *J. Raman Spectrosc.* **2002**, *33*, 238.

(28) Strano, M. S. *J. Am. Chem. Soc.* **2003**, *125*, 16148.

(29) Kotchey, G. P.; Gaugler, J. A.; Kapralov, A. A.; Kagan, V. E.; Star, A. *J. Mater. Chem. B* **2013**, *1*, 302.

(30) Weisman, R. B. *Anal. Bioanal. Chem.* **2010**, *396*, 1015.

(31) Maultzsch, J.; Telg, H.; Reich, S.; Thomsen, C. *Phys. Rev. B* **2005**, *72*, 205438.

(32) O'Connell, M. J.; Sivaram, S.; Doorn, S. K. *Phys. Rev. B* **2004**, *69*, 235415.

(33) Barros, E. B.; Filho, A. G. S.; Lemos, V.; Filho, J. M.; Fagan, S. B.; Herbst, M. H.; Rosolen, J. M.; Luengo, C. A.; Huber, J. G. *Carbon* **2005**, *43*, 2495.

(34) Martínez, M. *Carbon* **2003**, *41*, 2247.

(35) Strano, M. S.; Dyke, C. A.; Usrey, M. L.; Barone, P. W.; Allen, M. J.; Shan, H. W.; Kittrell, C.; Hauge, R. H.; Tour, J. M.; Smalley, R. E. *Science* **2003**, *301*, 1519.

(36) Graupner, R. *J. Raman Spectrosc.* **2007**, *38*, 673.

(37) Dyke, C. A.; Tour, J. M. *J. Am. Chem. Soc.* **2003**, *125*, 1156.

(38) Chiang, I. W.; Brinson, B. E.; Huang, A. Y.; Willis, P. A.; Bronikowski, M. J.; Margrave, J. L.; Smalley, R. E.; Hauge, R. H. *J. Phys. Chem. B* **2001**, *105*, 8297.
(39) Haggenmueller, R.; Rahatekar, S. S.; Fagan, J. A.; Chun, J.; Becker, M. L.; Naik, R. R.; Krauss, T.; Carlson, L.; Kadla, J. F.; Trulove, P. C.; Fox, D. F.; DeLong, H. C.; Fang, Z.; Kelley, S. O.; Gilman, J. W. *Langmuir* **2008**, *24*, 5070.
(40) Huang, L. S.; Colas, C.; Ortiz de Montellano, P. R. *J. Am. Chem. Soc.* **2004**, *126*, 12865.
(41) Liu, X.; Hurt, R. H.; Kane, A. B. *Carbon* **2010**, *48*, 1961.
(42) Cherukuri, T. K.; Tsyboulski, D. A.; Weisman, R. B. *ACS Nano* **2012**, *6*, 843.
(43) Boehm, H. P. *Carbon* **2002**, *40*, 145.
(44) O'Connell, M. J.; Eibergen, E. E.; Doorn, S. K. *Nat. Mater.* **2005**, *4*, 412.
(45) Kim, K. K.; Yoon, S.-M.; Park, H. K.; Shin, H.-J.; Kim, S. M.; Bae, J. J.; Cui, Y.; Kim, J. M.; Choi, J.-Y.; Lee, Y. H. *New J. Chem.* **2010**, *34*, 2183.
(46) Tanaka, Y.; Niidome, Y.; Nakashima, N. *Chem. Lett.* **2009**, *38*, 864.
(47) Sgobba, V.; Guldi, D. M. *Chem. Soc. Rev.* **2009**, *38*, 165.
(48) Nikolaev, P.; Bronikowski, M. J.; Bradley, R. K.; Rohmund, F.; Colbert, D. T.; Smith, K. A.; Smalley, R. E. *Chem. Phys. Lett.* **1999**, *313*, 91.
(49) Muramatsu, H.; Hayashi, T.; Kim, Y. A.; Shimamoto, D.; Kim, Y. J.; Tantrakarn, K.; Endo, M.; Terrones, M.; Dresselhaus, M. S. *Chem. Phys. Lett.* **2005**, *414*, 444.
(50) Ziegler, K. J.; Gu, Z. N.; Peng, H. Q.; Flor, E. L.; Hauge, R. H.; Smalley, R. E. *J. Am. Chem. Soc.* **2005**, *127*, 1541.
(51) Elstner, M.; Porezag, D.; Jungnickel, G.; Elsner, J.; Haugk, M.; Frauenheim, T.; Suhai, S.; Seifert, G. *Phys. Rev. B* **1998**, *58*, 7260.
(52) Lee, S. M.; An, K. H.; Lee, Y. H.; Seifert, G.; Frauenheim, T. *J. Am. Chem. Soc.* **2001**, *123*, 5059.
(53) Henkelman, G.; Uberuaga, B. P.; Jonsson, H. *J. Chem. Phys.* **2000**, *113*, 9901.